Asian Journal of Civil Engineering (2021) 22:1447–1460
https://doi.org/10.1007/s42107-021-00386-9

ORIGINAL PAPER

Seismic performance of RC frames under sequential ground motion

Athar Tauheed[1] · **Mehtab Alam**[1]

Received: 17 February 2021 / Accepted: 10 August 2021 / Published online: 5 September 2021

Abstract
The current practice of the seismic design of buildings relies on a single event of earthquake having a specified intensity measure. Two-level earthquakes are used along with the specified design response spectrum for arriving at the seismic design forces. The seismic performance of the designed structure is evaluated using non-linear time history analysis for some specified ground motion or synthetically generated ground motion from the response spectrum. No consideration is paid to the aftershock event, which is commonly associated with any major shock. The present study investigates the adequacy of the current design practice to cater to the aftershock events using 11-storey RC frame subjected to a sequence of main- and aftershocks synthetically generated from the design response spectrum as specified in the IS code. Several seismic demand parameters, namely, transient and residual top displacements, maximum inter-storey drift, residual storey drift, base shear and a number of plastic hinges, are used to evaluate the seismic performance of the frame for each earthquake shock. The result of the study indicates that with the increase in the number of aftershocks, significant deterioration of strength and stiffness takes place, resulting in the residual demand parameters exceeding the permissible limit.

Keywords Non-linear time history analysis · RC frame · Aftershocks · Synthetically · Seismic performance

Introduction

As per the prior experiences and studies, the majority of the earthquakes have a series of aftershocks after the strong mainshock, which follow it consecutively. It is generally observed that a strong mainshock is always accompanied by many aftershocks, out of which few seismic sequences may last for years altogether. These mainshock–aftershock sequences can lead to serious damage to structures, undermine life safety, and result in substantial economic losses even though the structure might have been only slightly damaged from the mainshock (Song et al., 2016). For example, two powerful earthquakes occurred on April 25, 2015 in Nepal. The first earthquake hits at 06:11 UTC with an intensity of 7.8 $M_{w,}$ 80 km to the NW of Kathmandu. The second earthquake took place at 06:45 UTC with an intensity of 6.6 M_w and its epicentre was at a distance of 65 km east of Kathmandu. The earthquakes were followed by 38 consecutive aftershocks of magnitude 4.5 M_w or greater throughout the day, amongst which the highest was of magnitude 6.8 M_w (2015). The intense Tohoku earthquake on March 11, 2011, in Japan, activated 60 aftershocks with M_w 6.0 or more and three with M_w 7.0. The aggregate monetary losses in Japan were assessed at US$309 billion. Damage might not be severe during the mainshock, but there could be a lack of repair due to time constraints or other reasons. Such a damaged structure may suffer severe damages or even collapse in the succeeding aftershocks. There is a decline in the strength as well as the stiffness of that structure that in turn leads to a decrease in capacity as a result of inter-storey drift increase (Hatzigeorgiou & Beskos, 2009; Hatzivassiliou & Hatzigeorgiou, 2015; Hosseinpour & Abdelnaby, 2017) during repeated ground motion in comparison of a single earthquake event. It is observed that in the case of repetitive ground motions, with each aftershock there is a continuous accumulation of residual displacement and storey drift and even the seismic demand is higher in comparison of a single episode of the earthquake and may lead to severe damages to buildings (Amadio et al., 2003; Hatzigeorgiou & Liolios, 2010; Abdelnaby & Elnashai, 2015).

✉ Athar Tauheed
athar.dce@gmail.com

Mehtab Alam
malam1@jmi.ac.in

[1] Department of Civil Engineering, Jamia Millia Islamia, Jamia Nagar, New Delhi 110025, India

The mainshock episode mostly governs seismic design and assessment of building frames. No code specifies directly in its recommendation the effect of aftershock in the seismic design. However, the same factor of safety is incorporated in the design to cater to the effect of the aftershock. In the past earthquake, it was observed that many seismically well-designed structures which stand the mainshock with stipulated damages failed to perform satisfactorily or collapsed during the aftershocks. This observation led to widespread research in the study of the effects of aftershocks in the seismic design of structures, especially the damage state evaluation after the mainshock. Thus, the behaviour of structures during the aftershocks formed a major topic of research.

Faisal et al. (2013) studied the effects of repeated ground motions on ductility demands of 3-, 6-, 12-, and 18-storey buildings having inelastic concrete frames. Empirical relationships were presented to estimate the maximum ductility demands of these multi-storeyed structures under the effect of succeeding earthquakes. Hatzigeorgiou and Liolios (2010) studied eight reinforced concrete frames' inelastic behaviour under repeated ground motions. Each regular and vertically irregular (3- and 8-storey buildings) were designed for both seismic and vertical load consecutively. It was concluded that the repetition of ground motion remarkably influenced the response and design of reinforced concrete frames. An empirical expression was proposed to calculate the ductility demand under the effect of repeated ground motions.

Hatzigeorgiou and Liolios (2015) investigated the inelastic response of three-dimensional reinforced concrete structures, both regular and irregular, subjected to five real strong sequential ground motions. They concluded that ductility demands increased in case of multiple ground motions compared to a single event of an earthquake. In another study, Hosseinpour and Abdelnaby (2017) studied the non-linear response of two regular and irregular (in height), eight-storey RC buildings subjected to repeated earthquakes. A conclusion was drawn that the effect of direction of earthquakes, aftershock polarity and the vertical component of the earthquake was more significant in irregular buildings than regular buildings.

Raghunandan et al. (2015) explained that if buildings exposed to sequential earthquakes were mildly damaged during the mainshock, they were likely to experience minimum damage aftershock events too. But if the damage was severe during the mainshock, the repercussion was severe during the aftershock events. It was concluded that the higher the drift experienced during the mainshock event, the more the chances of collapse during aftershock due to reduced collapse capacity of these ductile structures.

Hatzigeorgiou (2010) dealt with the ductility demand spectra under near- and far-fault sequential ground motions for single degree of freedom (SDOF) systems. The main intention of the study was the quantification of the seismic sequence effect directly in terms of ductility demands. Loulelis et al. (2012) had performed an extensive analysis on the plane moment-resisting frames subject to powerful seismic sequences. Due to negligible time available between two seismic events, the structure had no time to retrofit, leading to a remarkable damage accumulation in the buildings. A study had been carried out on 36 moment-resisting frames designed for seismic and vertical loads exposed to five multiple real earthquakes for up to 3 days. The frames were also subjected to 60 artificial sequential ground motions and reported that the sequences of the ground motions had a significant effect on the response and the design of the moment-resistant frames.

Zhai et al. (2013) dealt with the mainshock–aftershock sequence-type earthquakes and their damage spectra was calculated by Park–Ang damage index. The consequences of a period of vibration, damping ratio, seismic sequence, site condition, strength reduction factor and post-yield stiffness were studied with the help of statistics. The outcomes showed that the consequence of aftershocks was remarkable on structural damage. A simplified equation was proposed to simplify the application of damage spectra in the seismic practice for a mainshock–aftershock sequential earthquakes.

Zhai et al. (2014) studied the behaviour of the structure in active regions which were exposed to frequent mainshock–aftershock sequential earthquakes. With the help of the SDOF system having four hysteretic models, they studied three response demand parameters. The results indicated that the effect of the damage index and normalised hysteretic energy was more significant than the ductility demand in the case of aftershocks. The effects of the aftershock ground motion with larger PGA as/PGA ms on the response demand were generally more obvious for the non-degrading system than for the degrading system.

Kassem et al. (2019) extensively examined the seismic behaviours of one regular frame along with nine setback frames of varying building configurations of a six-storey moment-resisting concrete frame. Using three sets of sequential earthquake records, incremental dynamics analysis (IDA) was conducted. As per the IDA curve, fragility curves were developed using the life safety (LS) performance level as the main guideline. The lowest probability was exhibited by the regular frame in comparison to others. The building's seismic performance was affected by the configuration of frames and was considered in the seismic design of buildings.

Oyguc et al. (2018) investigated the three plan asymmetric RC structures that had been subjected to the powerful Tohoku seismic sequences taking into consideration the performance of the structures under them. An inference drawn stated that there was an increase in the residual drift demands in the case of irregular RC buildings due to

the structural irregularity compared to regular RC structures. In another study, Tolentino et al. (2018) proposed an approach to describe the evolution of damage that a structure could accumulate by the action of seismic sequences at the end of a time interval. They used a damage index that quantified the cumulative damage. The index considered both the demanded drift and ultimate drift. Using this proposal, they also obtained the structural reliability expressed in terms of reliability functions.

Parekar et al. (2020) studied the disastrous effects of sequential earthquakes on buildings that are located in earthquake-prone areas. Such buildings have no time left for rehabilitation after the mainshocks and hence the aftershocks have proven to be fatal for them. They evaluated the seismic demands in terms of IDR for these 3-, 6-, and 9-storeyed SMRF structures and examined the consequences of repetitive ground motions on them. It was concluded that there was an unusual influence on these irregular structures (irregularity introduced along with the height at different storeys), especially due to the aftershocks. Higher seismic demand was reported with irregularity at the bottom than it was in other storeys.

Hassan et al. (2020) investigated three semi-rigid frames having connection capacities as 50%, 60% and 70% of the plastic moment of the beam. They were assessed under the influence of sequential ground motions. Two types of analyses—push over analysis and non-linear time-history analyses—were conducted on them and the outcomes showed an increment in the probability of attaining or going beyond a particular damage limit state in the frames when the aftershocks were included. Sharma et al. (2021) performed a probabilistic seismic evaluation with the help of fragility analysis on a ten-storey semi-rigid steel frame exposed to both near and far-field earthquakes. It was inferred that there is a considerable impact on the probability of exceedance compared to the far-field earthquake due to the high directivity ratio of the near-field earthquake.

Sharma et al. (2020) examined the seismic behaviour of steel frames (five-storey and ten-storey) that are semi-rigid in nature and subjected under the influence of near and far-field earthquakes. The conclusion drawn from the analysis exhibited that the semi-rigid frames turn out to be more effective and efficient in resisting the seismic forces of near-field earthquakes (PGA = 0.2 g). Mohsenian et al. (2021) investigated the 4-, 8- and 12-storey eccentrically braced steel frame buildings to examine the effect of mainshock and aftershock sequences on them with energy-absorbing links. Bhandari et al. (2018) examined the behaviour of base-isolated building frames with the help of a numerical study for far-field and near-field earthquakes with directivity and fling-step effects. It was concluded that the base isolation is not effective in case of near-field earthquakes.

It is evident from the above review of literature that behaviour of building frames under multiple aftershocks is not well investigated. Most of the studies consider the effect of a single aftershock after the mainshock. Further, damage states (performance levels) after the mainshock and each aftershock are not critically evaluated, especially in terms of the residual and peak damages during and after each mainshock. With this background in view, the present study is undertaken. An 11-storey building frame seismically designed according to the Indian standard code provision is subjected to the sequence of a mainshock followed by several aftershocks. The sequence is synthetically generated from the IS compatible response spectrum. The performance behaviour is measured in terms of well-documented threshold values of some critical seismic demand measures at every episode and after the end of the episode.

Theory

A 2D model of a typical RC frame of 11-storey building is used in the study. A lumped mass matrix is used with masses lumped at different storeys. The damping matrix is defined as a classically damped Rayleigh's damping matrix $C = \alpha 1M + \alpha 2K$, where α1 and α2 are real scalars. The frame is assumed to yield at each end section of the columns and beams. The backbone curves of the yield hinges are taken as the default hinge property provided in SAP (2000). The incremental dynamic equation of motion is solved using the Hilber–Hughes–Taylor integration (HHT) scheme (Attili, 2010). Alpha (α) is the only parameter that is being used in the HHT method. It takes up values between 0 and − 1/3. When we take alpha equal to zero ($\alpha = 0$), it is seen that this method becomes equivalent to the Newark-beta method where the value of beta is taken as 0.25 and the value for gamma is taken as 0.5. Hence, it becomes similar to the average acceleration method. The accuracy is seen at its highest amongst the available methods when the value for alpha is taken as 0. However, there is permission for excessive vibrations observed in the modes having a higher frequency. These modes are seen to have periods of the same order as or less in value of time step size. Severe damping is exhibited at higher frequency modes for more negative values that are obtained for alpha. Since smaller time steps are being considered, this is not considered as physical damping. It becomes essential to use a negative value of alpha to encourage a non-linear solution to converge. To obtain the best results, it becomes imperative to consider the smallest time step in the most practical aspect possible, and the alpha value should be taken closest to the value of zero.

The effect of aftershock is included in the analysis by joining the time histories of accelerations, starting from the mainshock included in the study by joining the time history

record of the mainshock with those of the subsequent aftershocks in series with sufficient gaps provided with zeros so that the structure comes to the condition of rest before the next episode acts on to it.

Numerical study

Asymmetrical 11-storey reinforced concrete square building consisting of four bays in each direction of 5 m width and floor to floor height as 3.2 m is considered as an illustrative example (Fig. 1B). The middle frame of the building is selected as shown in Fig. 1A. The building is located in high seismic zone (zone V) according to IS 1893:2000, and is designed as per Indian standard code (2002, 2002, 2016). The middle frame of the building is selected for the analysis. The dead load (gravity load) is 12.5 kN/m and live load is 5 kN/m with live load of roof as 3.75 kN/m. The thickness of the wall is 115 mm and load is 6.75 kN/m. Other material properties are assumed to be 25 MPa for concrete compressive strength (concrete grade M25) (Mander et al., 1988) and 415 MPa and 500 MPa for the yield strength of transverse and longitudinal steel (Park and Ang, 1985). The degradation under cyclic loading is incorporated using the Takeda hysteresis model in the SAP2000 software, as shown in Fig. 1C. The size of the column is 450 mm × 450 mm, and beams' size is 230 mm × 450 mm. The base of the frame is assumed to be fixed. The nonlinearity of the frame is introduced by lumped plasticity by defining plastic hinges at both the ends of beams and columns according to FEMA 356 (1997, 2000, 2009). Force–deformation behaviour of plastic hinge is described by five points A, B, C, D, and E and three additional points between B and C are labelled as IO (Immediate Occupancy), LS (life safety) and CP (collapse prevention) are used to define the acceptance criteria for the hinge as shown in Fig. 1D. To examine and compute the non-linear behaviour of the structure, default frame hinges are described for columns and beams as per FEMA 356 in SAP2000 (SAP, 2000 2016).

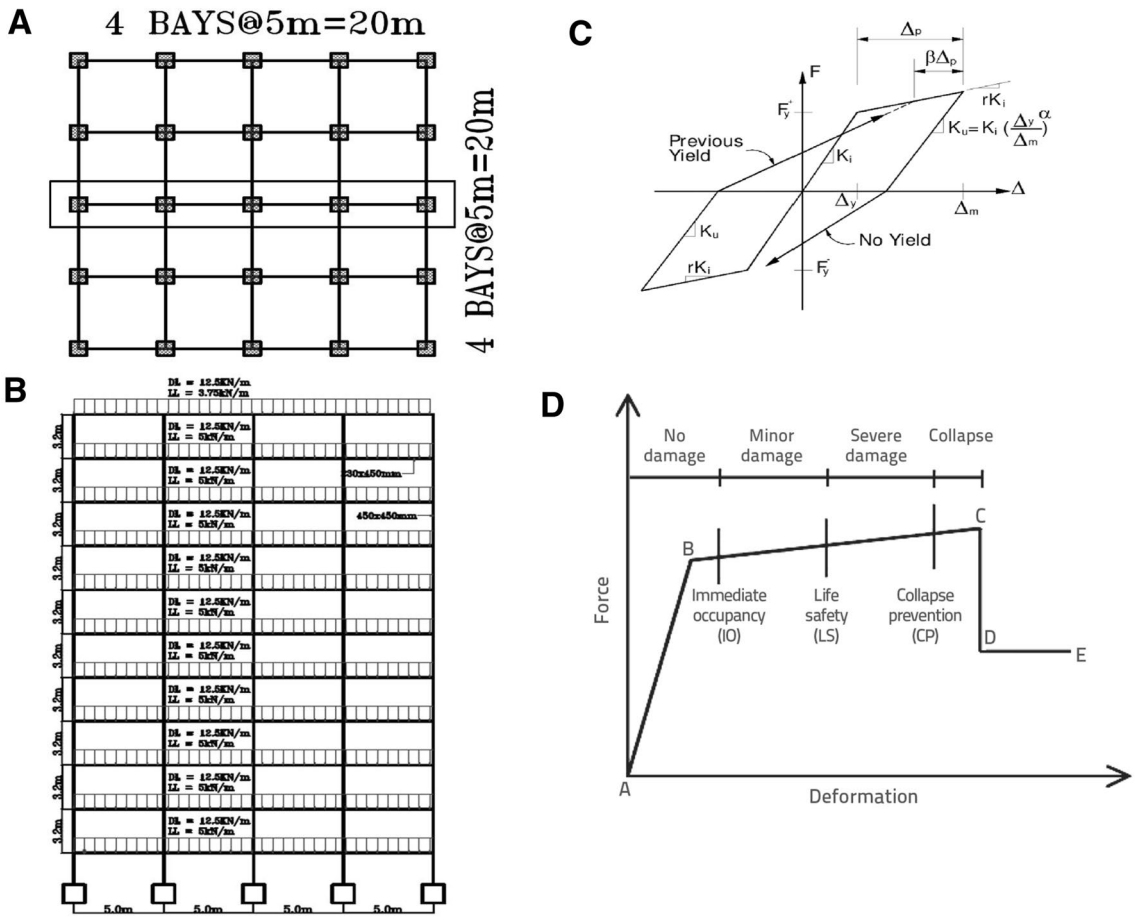

Fig. 1 **A** Plan view of the building, **B** elevation detail of 11-storey RC regular frame. **C** Takeda hysteresis model (Takeda et al., 1970). **D** Force–deformation relationship of a typical plastic hinge (structural performance levels) (Erdem, 2016)

Sequential ground motion

The ground motion inputs are the response spectrum (IS1893:2000) compatible scaled time history of ground motion artificially generated using the standard software Seismo-Signal (SeismoSoft., 2020) as per Table S1. The ground motion is scaled to five different PGAs (0.36 g, 0.4 g, 0.45 g, 0.5 g, and 0.55 g) as mainshocks. The aftershock PGA is calculated as two-thirds of the mainshock PGAs. The effect of the aftershock is considered by joining aftershocks and the mainshock sequentially, as discussed before. Mainshock and six aftershocks are sequentially joined one after another to form the sequence of earthquake events. The formation of the sequence of earthquake events is shown in Fig. 2.

Results and discussion

The regular frame as shown in Fig. 1 is taken as an example for the non-linear time history analysis under repeated ground motions having five mainshocks of PGAs (0.36 g, 0.4 g, 0.45 g, 0.5 g, and 0.55 g). Six aftershocks follow each mainshock. The intensity of each aftershock is taken as two-thirds of the mainshock. The response quantities of interest include the maximum transient, residual top floor displacements, and inter-storey drift. Apart from these two important responses, the maximum base shear and the number of plastic hinges formed in the mainshock and each aftershocks are determined.

Maximum transient top floor horizontal displacement

Transient top floor displacement for sequential ground motion with 0.36 g (Case1) and 0.45 g (Case2) PGAs as mainshocks is shown in Fig. 3A, B. It is observed from the figures that the maximum transient top horizontal

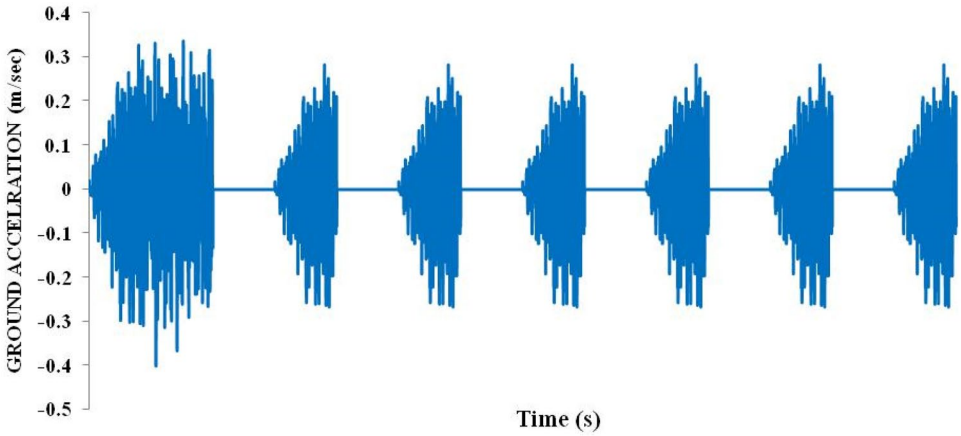

Fig. 2 Time history compatible to IS1893:2016

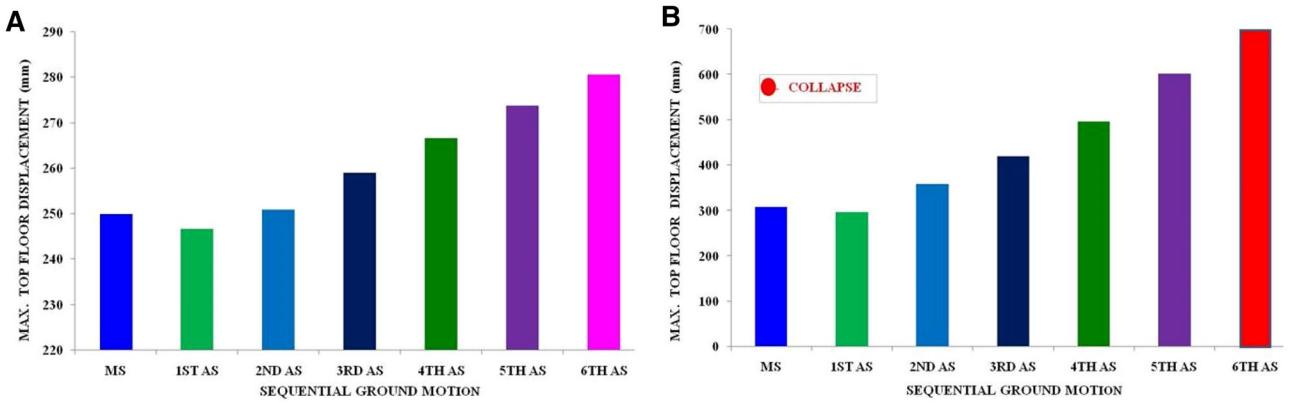

Fig. 3 Maximum transient top floor displacement: **A** Case1—Table 1, and **B** Case3—Table 2

Table 1 Drift ratio at the threshold value of structural damage (HAZUS MR4 (2017))

Slight	Moderate	Extensive	Collapse
0.0025	0.0045	0.0115	0.03

displacement increases with the increase of the number of aftershocks except for the first aftershock. Since the aftershock has less intensity than the mainshock, it is expected to have less maximum transient top storey displacement in the aftershock if it started with zero initial condition. However, the oscillation in the aftershock starts with a residual displacement, and therefore, the maximum transient top storey displacement in the aftershock depends on the value of the initial displacement. In the present problem, the value of the residual displacement after the mainshock is not significantly large. Consequently, the transient displacement in the first aftershock does not become more than that of the mainshock. With subsequent aftershocks, the residual displacement increases, leading to increased transient top storey displacements in subsequent aftershocks, as shown in Fig. 4. Note that a distinct increase of residual displacement in the figure is visible only after 3 or 4 aftershocks. This is the case because there is an accumulation of the permanent displacement after each aftershock leading to the final top floor displacement. However, it may be noted that the maximum transient top storey displacement decreases in the first aftershock for all cases, as shown in Table 1. The reason for this has been described before. Further, it may be noted that the transient top storey displacement reaches very high value for some cases so that the program fails to execute beyond the previous aftershock showing failure of the structure. This shows that the aftershock effect could be highly significant.

Table 2 Maximum transient top floor displacement for sequential ground motion (Case1–Case5)

	Maximum transient top floor displacement (mm) for PGA				
	0.36 g as mainshock (Case1)	0.40 g as mainshock (Case2)	0.45 g as mainshock (Case3)	0.50 g as mainshock (Case4)	0.55 g as mainshock (Case5)
Mainshock	249.8	274.1	307.4	346.9	399.1
First aftershock	246.6	271.3	296.1	315.3	342.9
Second aftershock	250.8	296	358.1	397.6	450.3
Third aftershock	258.9	321.1	418.8	508.3	601.8
Fourth aftershock	266.6	346	495.1	655.3	Collapse
Fifth aftershock	273.7	372.3	601.5	Collapse	Collapse
Sixth aftershock	280.5	401.7	Collapse	Collapse	Collapse

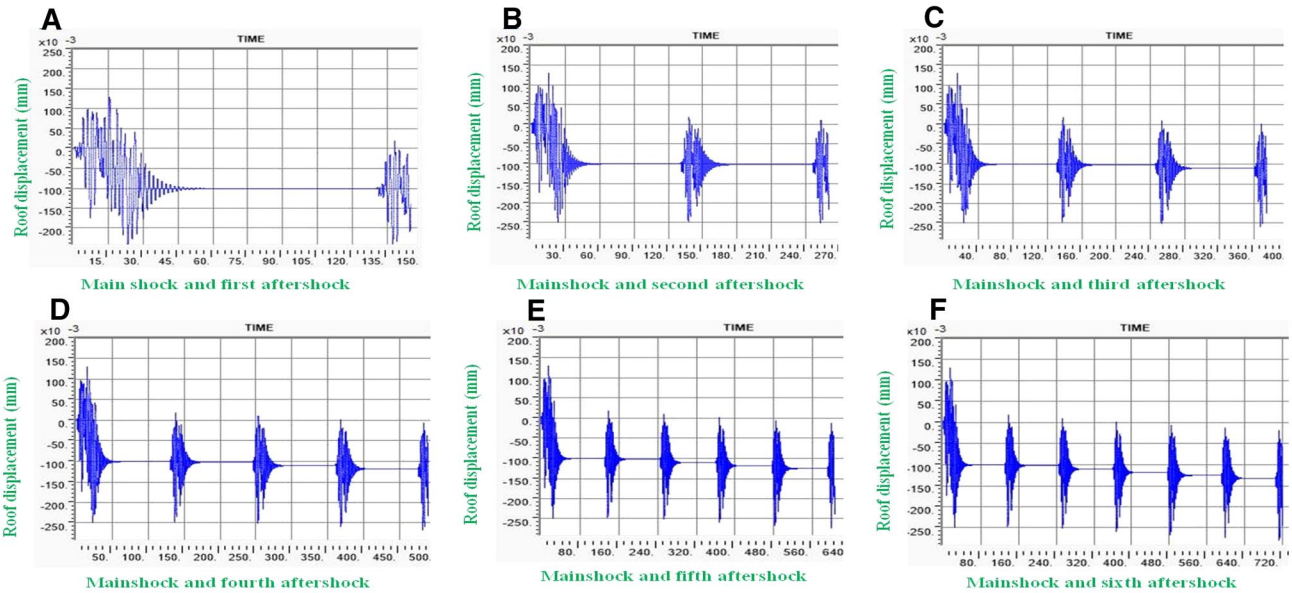

Fig. 4 Typical time history of top horizontal displacement under repeated ground motion with PGA as 0.36 g

Maximum residual top floor displacement

From Fig. 5A, B, it is observed that the residual top storey displacement, like transient maximum top storey displacement, increases with the number of aftershocks. The increase is clearly due to the accumulation of the residual displacements as the aftershocks are applied one after another. It is seen from Table 3 that as the PGA of the mainshock is increased, the residual displacements at the fifth aftershock increase. For the last two cases of the PGA, the residual displacements become so large that they destabilise the system. Thus, in terms of residual displacement, the effect of the aftershock could be highly significant and deserves attention in the design.

Maximum transient storey drift

Figure 6A, B shows maximum transient storey drift in the mainshock and at each aftershock. It is seen that the storey drift increases with the number of aftershocks. For case B, the storey drift exceeds the limiting value of the drift at the last aftershock as per Table 1. The increase of storey drift is the same as that for the increase of top storey displacement with the number of aftershocks. The storey drifts for the five cases are shown in Table 4. It is seen from the table that the storey drifts increase with the increase in the PGA of the mainshock as to be expected. The storey at which the maximum drift is observed is shown in the bracket in each column. It may be observed from the table that the storey, in which the maximum storey drift occurs, does not remain the same in each aftershock. It changes with the number of aftershocks.

Further, it is observed from the table that from the case third onwards, the storey drift exceeds the limiting value after certain aftershock. In terms of the maximum storey drift, the aftershock effect is of the same importance as the top storey displacement. The building is vulnerable to aftershock both in terms of top storey displacement and storey drift.

Maximum residual storey drift

Maximum residual storey drift after the mainshock and after each aftershock is shown in Fig. 7A, B. It is seen from the figures that, like the transient maximum drift, the maximum residual drift increases with the number of aftershocks.

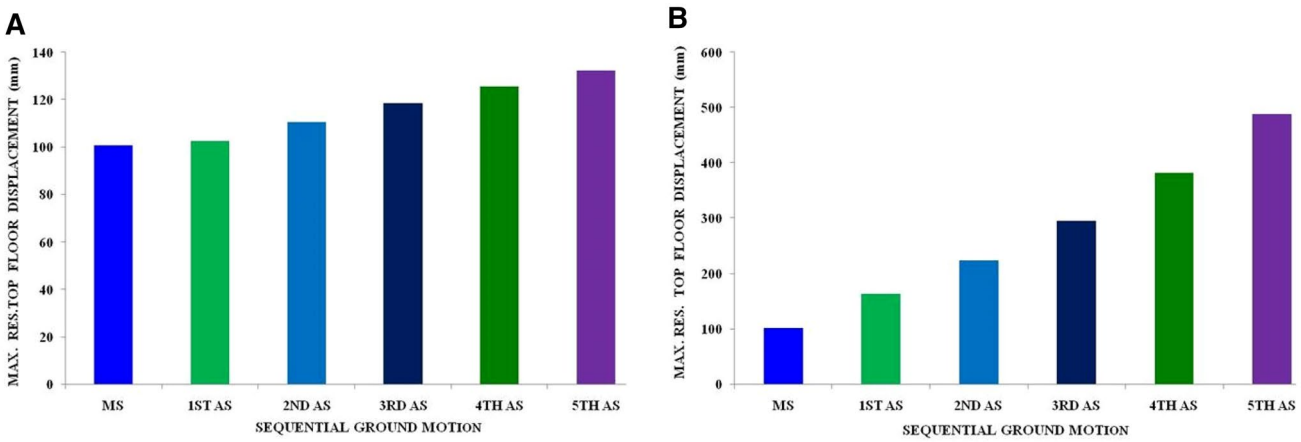

Fig. 5 Maximum residual top floor displacement for sequential ground motion **A** Case1—Table 2 **B** Case3—Table 2

Table 3 Maximum residual top floor displacement for sequential ground motion (Case1–Case5)

	Maximum residual top floor displacement (mm) for PGA				
	0.36 g as mainshock (Case1)	0.40 g as mainshock (Case2)	0.45 g as mainshock (Case3)	0.50 g as mainshock (Case4)	0.55 g as mainshock (Case5)
Mainshock	100.7	104.1	100.9	93.49	92.63
First aftershock	102.4	127	162.9	186.3	216.2
Second aftershock	110.5	152.1	223.8	276	330.4
Third aftershock	118.3	177.3	294.7	392.3	485
Fourth aftershock	125.4	203.8	380.9	539.9	Collapse
Fifth aftershock	132.2	233.3	487.3	Collapse	Collapse

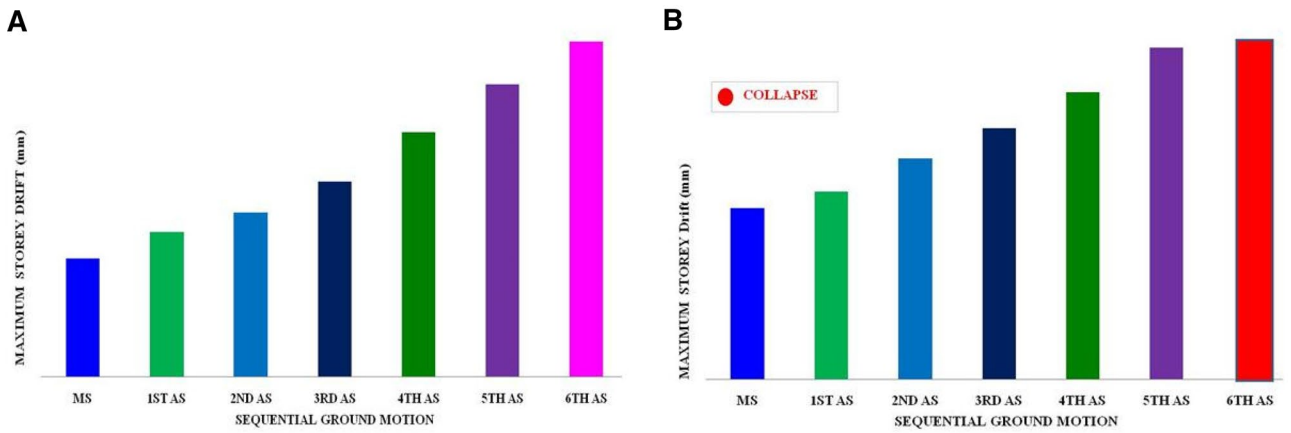

Fig. 6 Maximum transient storey drift for sequential ground motion: **A** Case1, **B** Case3

Table 4 Maximum transient storey drift for sequential ground motion (Case1–Case5)

	Maximum transient storey drift (mm) for PGA				
	0.36 g as mainshock (Case1)	0.40 g as mainshock (Case2)	0.45 g as mainshock (Case3)	0.50 g as mainshock (Case4)	0.55 g as mainshock (Case5)
Mainshock	31.7 6th storey	34.8 6th storey	38 3rd storey	44.5 4th storey	53.8 3rd storey
First aftershock	32.32 3rd storey	37.55 3rd storey	41.67 3rd storey	45.7 3rd storey	51.5 3rd storey
Second aftershock	32.75 4th storey	39.9 3rd storey	49.1 3rd storey	55.6 3rd storey	64.4 3rd storey
Third aftershock	33.46 4th storey	42.58 3rd storey	55.8 3rd storey	65.8 3rd storey	77.5 3rd storey
Fourth aftershock	34.59 4th storey	45.8 4th storey	63.8 3rd storey	79.5 3rd storey	Collapse
Fifth aftershock	35.69 4th storey	49.1 4th storey	73.7 3rd storey	Collapse	Collapse
Sixth aftershock	36.66 4th storey	52.7 4th storey	Collapse	Collapse	Collapse

Except for the first case, the steepness of the increase of the residual drift with the number of the aftershock increases with the increase of the PGA as evident from Table 5. Further, it is seen from the table that the residual drift exceeds the permissible limit for the higher value of the PGA at the fourth and fifth aftershock. Thus, residual drift also could be of concern in the case of aftershocks being encountered in sequence with mainshock.

Maximum base shear

The maximum base shears developed in the building frame during the main- and aftershocks are shown in Table 6. It is seen from the table that the maximum base shear in the mainshock increases with the increase of the PGA. The increase is not uniform. For the higher values of the PGA, the increase is a little more than the lower values of the PGA. This is the case because, with increasing PGA, the frame enters into a more inelastic state, requiring more lateral force. Further, it is seen from the table that with the number of aftershocks, the base shear decreases. This is the case because the overall stiffness of the frame decreases as a greater number of plastic hinges are formed with an increasing number of aftershocks. The decrease is more for the case of a mainshock with a high PGA value.

Force deformation curve

Figure 8A–E shows the typical plots of the force–displacement behaviours under different PGAs of earthquakes

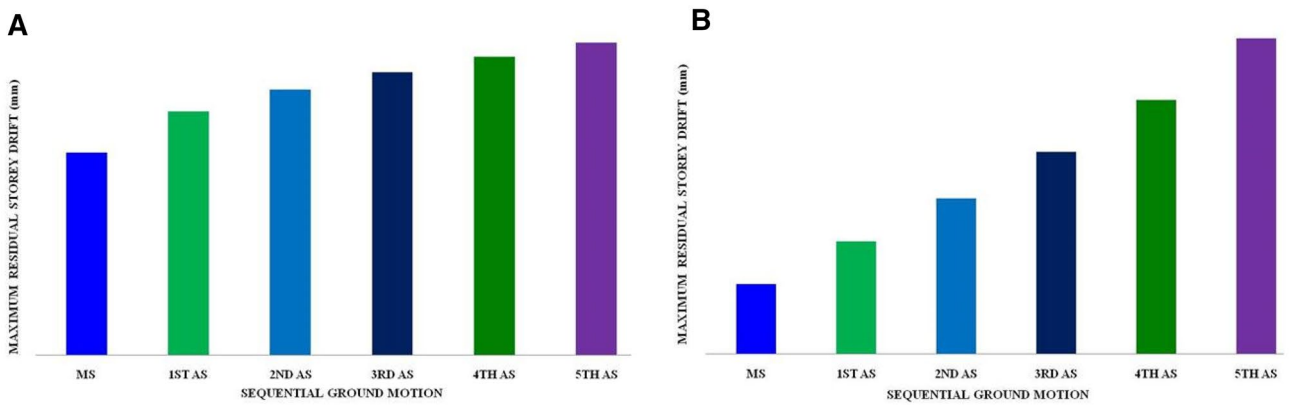

Fig. 7 Maximum residual storey drift for sequential ground motion: **A** Case1, and **B** Case3

Table 5 Maximum residual storey drift (Case1–Case5)

	Maximum residual storey drift (mm) for PGA				
	0.36 g as mainshock (Case1)	0.40 g as mainshock (Case2)	0.45 g as mainshock (Case3)	0.50 g as mainshock (Case4)	0.55 g as mainshock (Case5)
Mainshock	14.76 7th storey	14.28 7th storey	14.04 8th storey	13.32 8th storey	13.21 1st storey
First aftershock	17.76 6th storey	19.76 6th storey	22.5 6th storey	25.2 5th storey	16.69 5th storey
Second aftershock	19.37 6th storey	23.96 6th storey	31.1 6th storey	37 5th storey	24.76 5th storey
Third aftershock	20.64 6th storey	27.87 6th storey	40.3 6th storey	51.3 5th storey	40.02 5th storey
Fourth aftershock	21.74 6th storey	33.5 6th storey	50.7 6th storey	68.5 4th storey	Collapse
Fifth aftershock	22.78 6th storey	36 6th storey	63 6th storey	Collapse	Collapse

Table 6 Maximum base shear for sequential ground motion (Case1–Case5)

	Maximum Base shear (kN) for PGA				
	0.36 g as mainshock (Case1)	0.40 g as mainshock (Case2)	0.45 g as mainshock (Case3)	0.50 g as mainshock (Case4)	0.55 g as mainshock (Case5)
Mainshock	758.1	783.6	802.8	841.7	873.9
First aftershock	697.8	726	765.6	794.4	830.2
Second aftershock	705.3	728.4	770.4	811.8	836
Third aftershock	706.7	729.8	774.6	814.9	859.1
Fourth aftershock	706.6	731.2	788	845.8	Collapse
Fifth aftershock	706.5	733	811.4	Collapse	Collapse
Sixth aftershock	706.4	739.6	Collapse	Collapse	Collapse

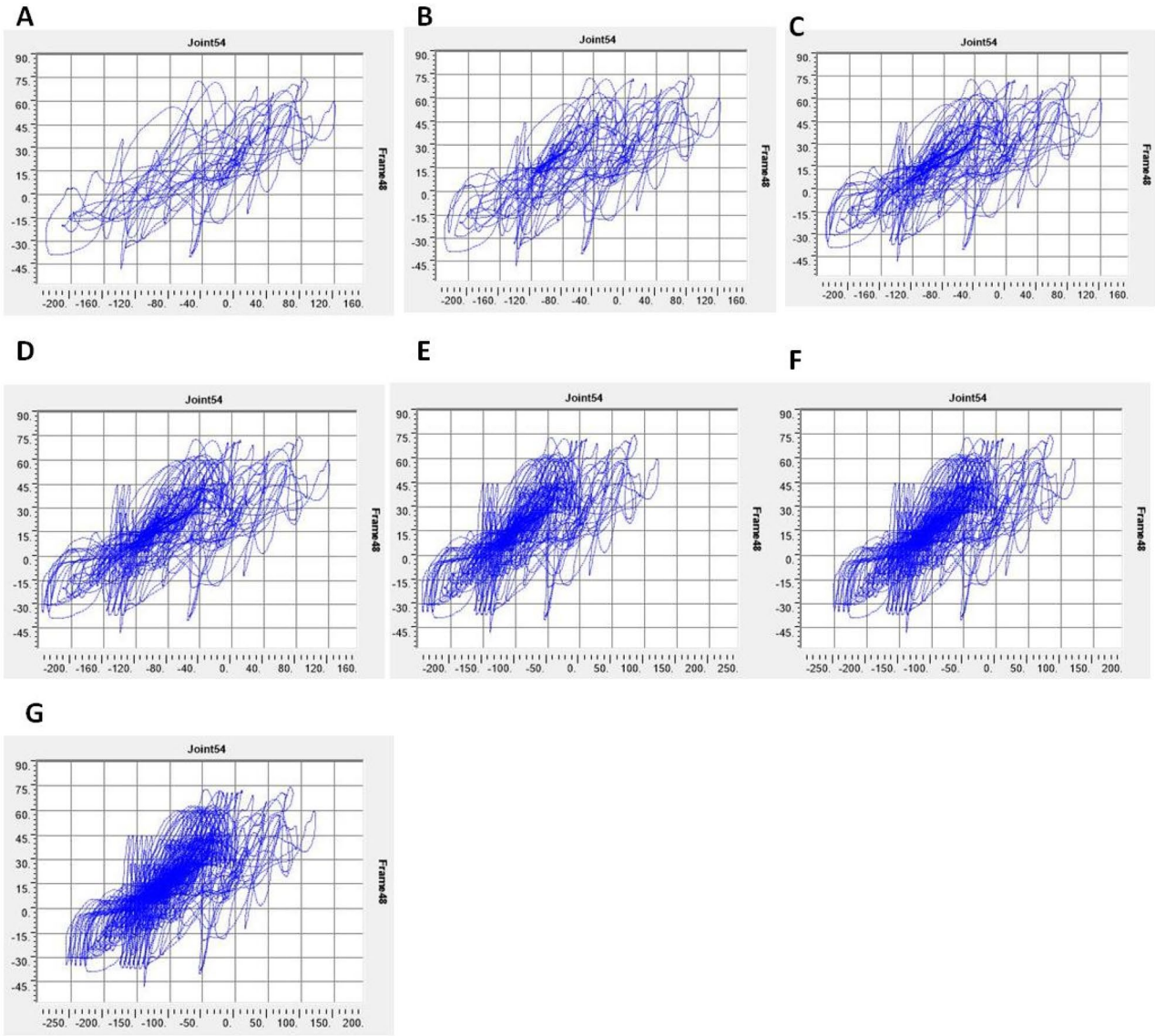

Fig. 8 Force deformation curves for Case1 **A** mainshock, **B** mainshock and first aftershock, **C** mainshock and second aftershock, **D** mainshock and third aftershock, **E** mainshock and fourth aftershock, **F** mainshock and fifth aftershock, **G** mainshock and sixth aftershock

which are compatible to IS1893:2016. It is seen from the figures that force–displacement characteristics are different for different PGA levels. It is observed that in the successive aftershocks following the mainshock, the number of hysteresis cycles within the loop goes on increasing, as depicted in Fig. 8. The hysteresis loop area widens at the higher value of PGAs as shown in Fig. 9 and the maximum displacement increases.

Formation of plastic hinges

According to FEMA's classification, different types of plastic hinges are formed during the mainshock and aftershocks. Figure 10 shows the plastic hinges formed in the frame in the sixth aftershock for all five cases. Table 7 provides the details of the plastic hinges formed in the frame for all five cases. It is seen from the table that the total number of plastic hinges formed in the frame increases with the level of the PGA as to be expected. The number of plastic hinges

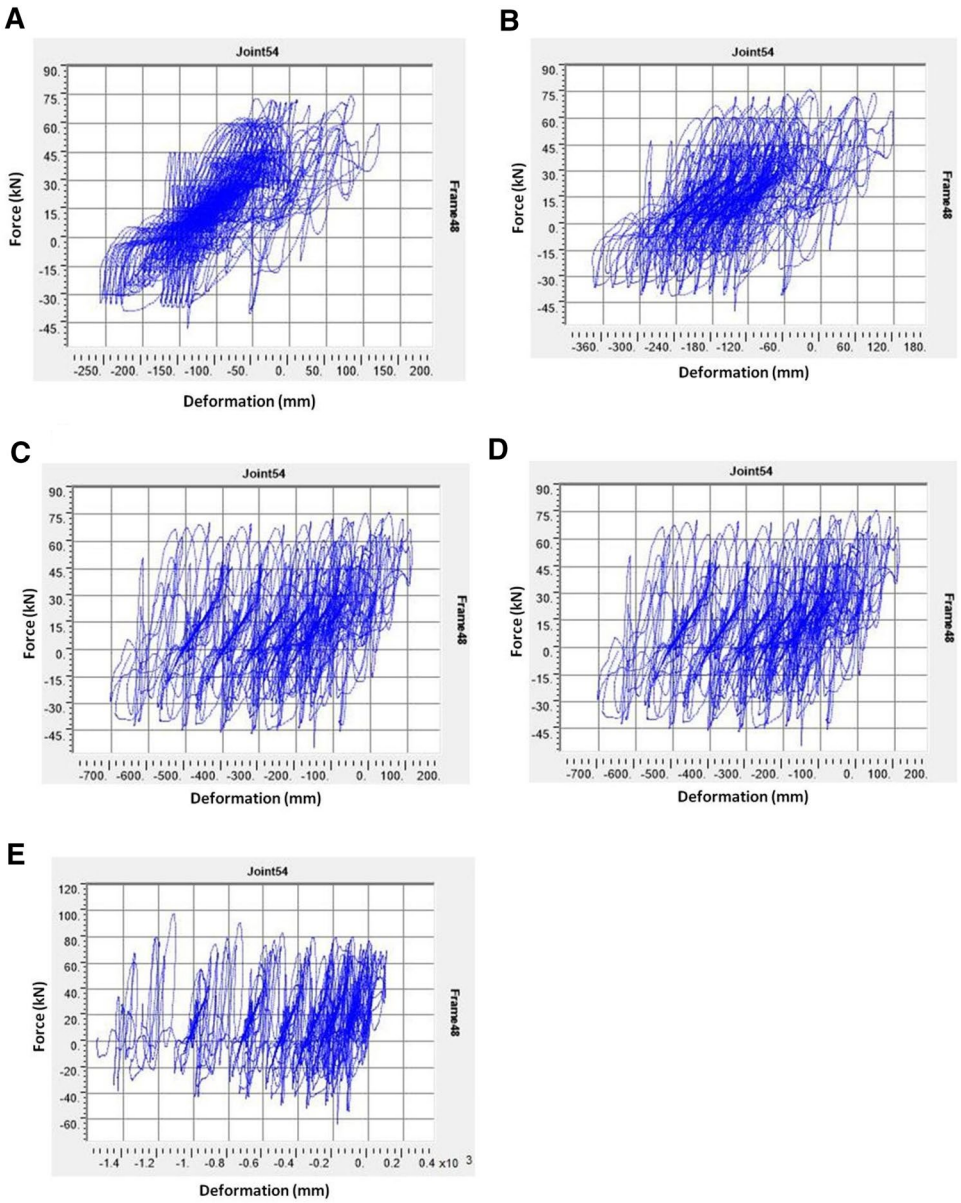

Fig. 9 Force deformation curves for **A** Case1, **B** Case2, **C** Case1, **D** Case4, and **E** Case5

going into higher plastic state (like LS-CP) also increases with the PGA level.

Further, the total number of plastic hinges formed due to each aftershock increases as the PGA increases. In the first case, there is no change in plastic hinges with the increase in the number of aftershocks. However, some of the hinges get their status changed with the aftershock. As the PGA increases, the total number of plastic hinges formed in the frame increases with the number of plastic hinges and the status of more hinges changes. For example, there is an increase in the number of plastic hinges at the sixth aftershocks for the last two cases to the tune of 16% and 30%, respectively. For these two cases, a large number of plastic hinges go into the level C–D. In addition, many plastic hinges go to the level of CP and beyond after the fourth aftershock.

Thus, the damageability of the frame significantly increases with several aftershocks, especially at higher PGA levels and the frames may be damaged to the extent that they may not be retrofitted. The effect of aftershocks in the seismic design of the frame needs to be considered from the point of safety of the design at the design level earthquake

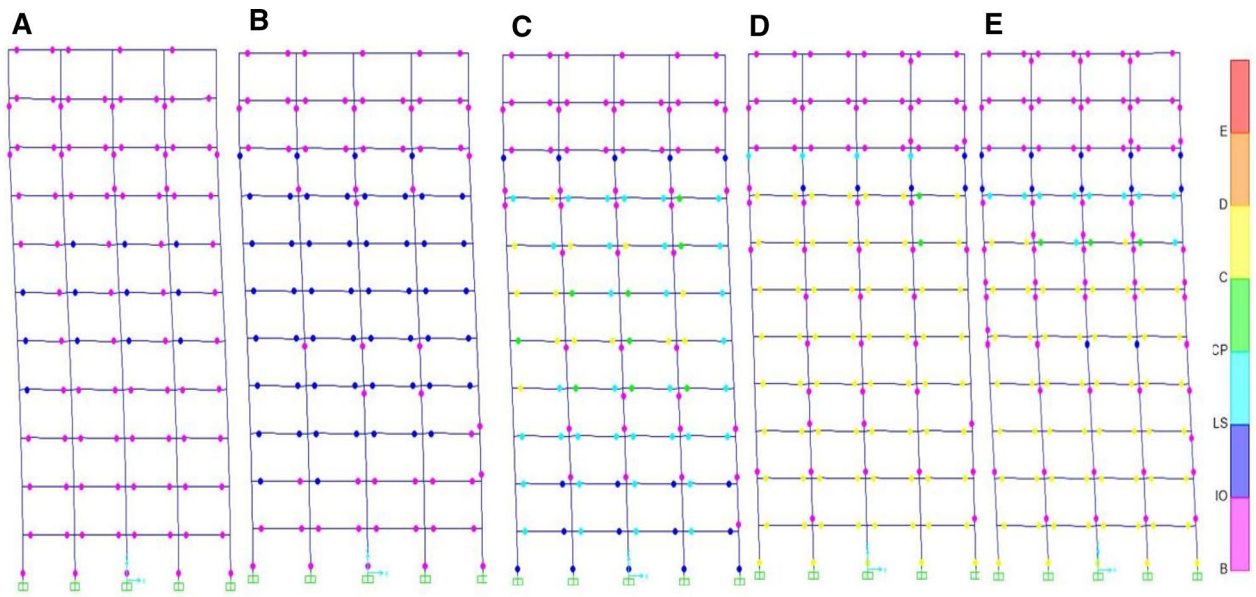

Fig. 10 Hinge pattern under mainshock and its aftershocks for **A** Case1, **B** Case2, **C** Case3, **D** Case4, and **E** Case5

and the extent of damage that might occur in the extreme level earthquake.

Conclusions

The response behaviour of multi-storey building frames under the mainshock and a series of aftershocks are investigated by performing a non-linear time history analysis in the SAP 2000. Five different levels of PGA, starting from 0.36 to 0.55 g are considered as the mainshocks. For each level of the mainshock, a series of six aftershocks are applied, each having a PGA of two-thirds the PGA of the mainshock. The response behaviour of the frame after the mainshock and subsequent aftershocks is investigated with the help of several response parameters. They include the maximum transient and residual top storey displacement, maximum transient and residual inter-storey drift, base shear and the number of plastic hinges formed. The numerical study leads to the following conclusions:

- Due to the deterioration of stiffness and strength under the influence of every aftershock, residual displacement is found, which goes on accumulating subsequently. At lower PGAs (0.36 g, 0.4 g, 0.45 g), the value of the cumulative residual displacement is within the permissible limits. Hence, the building survives. On the other hand, as the PGAs increase as seen in (0.5 g, 0.55 g), it crosses the permissible limit and results in the collapse of the structure.
- The same observations as above hold for the maximum inter-storey drift. Further, the storey in which the maximum inter-storey drift occurs might shift with the number of aftershocks.
- The frame survives the earthquake when the value of the base shear for the aftershock is either less than or approximately equal to the value of the base shear for the mainshock, else it collapses.
- The frame gets into the moderate inelastic state after the mainshock, even for the lower value of PGAs (0.36 g and 0.4 g). With the number of aftershocks, the increase in the plastic hinges is not very significant. However, the status of the plastic hinges is changed with the number of aftershocks.
- The frame undergoes significant inelastic actions developing plastic hinges beyond the status B for the higher level of PGAs (0.45 g, 0.5 g, 0.55 g). With aftershocks, there is an increase in the number of plastic hinges and considerable change in the status of the hinges. Some of the hinges cross the CP state showing the collapse in aftershock.
- The aftershock effect appears to be significant in terms of the accumulation of deformation and damages, leading even to collapse if the number and PGA level of the aftershocks are high.

Table 7 Total number of plastic hinges and their classification sequential ground motion

Events/performance	Mainshock	First aftershock	Second aftershock	Third aftershock	Fourth aftershock	Fifth aftershock	Sixth aftershock
Case1							
B-IO	102	101	101	97	93	93	89
IO-LS	–	–	–	4	8	8	12
Total no. of hinge	101	101	101	101	101	101	101
Case2							
B-IO	92	85	83	80	73	64	59
IO-LS	11	18	20	25	34	45	53
Total no. of hinge	103	103	103	105	107	109	112
Case3							
B-IO	85	83	64	51	43	49	53
IO-LS	22	24	45	61	47	41	18
LS-CP	–	–	–	–	23	33	34
CP-C	–	–	–	–	–	–	9
C-D	–	–	–	–	–	–	13
Total no. of hinge	107	107	109	112	113	123	127
Case4							
B-IO	78	74	61	56	58	61	61
IO-LS	40	44	61	46	27	9	5
LS-CP	–	–	–	24	47	18	4
CP-C	–	–	–	–	–	2	2
C-D	–	–	–	–	–	45	67
Total no. of hinge	118	118	122	126	132	135	139
Case5							
B-IO	71	71	68	68	70	73	76
IO-LS	55	57	55	42	11	7	13
LS-CP	–	–	14	32	21	4	4
CP-C	–	–	–	–	2	1	–
C-D	–	–	–	–	42	68	69
Total no. of hinge	126	128	137	142	146	153	162

Supplementary Information The online version contains supplementary material available at https://doi.org/10.1007/s42107-021-00386-9.

Acknowledgements The authors sincerely acknowledge Jamia Millia Islamia for funding and infrastructure support.

References

Abdelnaby, A. E., & Elnashai, A. S. (2015). Numerical modeling and analysis of RC frames subjected to multiple earthquakes. *Earthquakes and Structures, 9*(5), 957–981.

Amadio, C., Fragiacomo, M., et al. (2003). The effects of repeated earthquake ground motions on the non-linear response of SDOF systems. *Earthquake Engineering & Structural Dynamics, 32*(2), 291–308.

Attili, B. S. (2010). The Hilber–Hughes–Taylor-α (HHT-α) method compared with an implicit Runge–Kutta for second-order systems. *International Journal of Computer Mathematics, 87*(8), 1755–1767.

Bhandari, M., Bharti, S., et al. (2018). The numerical study of base-isolated buildings under near-field and far-field earthquakes. *Journal of Earthquake Engineering, 22*(6), 989–1007.

Erdem, R. T. (2016). Performance evaluation of reinforced concrete buildings with softer ground floors. *Građevinar, 68*(01), 39–49.

Faisal, A., Majid, T. A., et al. (2013). Investigation of storey ductility demands of inelastic concrete frames subjected to repeated earthquakes. *Soil Dynamics and Earthquake Engineering, 44*, 42–53.

Federal Emergency Management Agency (FEMA) (2017) Hazus 4.0. Washington, DC.

FEMA-273. (1997). *NEHRP Guidelines for Seismic Rehabilitation of Buildings*. Building Seismic Safety Council FEMA.

FEMA-356. (2000). *Prestandard and Commentary for the Seismic Rehabilitation of Buildings*. Federal Emergency Management Agency.

FEMA-P695. (2009). Quantification of Building Seismic Performance Factors. Federal Emergency Management Agency, FEMA-P695

Hassan, E. M., Admuthe, S., et al. (2020). Response of semi-rigid steel frames to sequential earthquakes. *Journal of Constructional Steel Research, 173*, 106272.

Hatzigeorgiou, G. D. (2010). Ductility demand spectra for multiple near-and far-fault earthquakes. *Soil Dynamics and Earthquake Engineering, 30*(4), 170–183.

Hatzigeorgiou, G. D., & Beskos, D. E. (2009). Inelastic displacement ratios for SDOF structures subjected to repeated earthquakes. *Engineering Structures, 31*(11), 2744–2755.

Hatzigeorgiou, G. D., & Liolios, A. A. (2010). Non-linear behaviour of RC frames under repeated strong ground motions. *Soil Dynamics and Earthquake Engineering, 30*(10), 1010–1025.

Hatzivassiliou, M., & Hatzigeorgiou, G. D. (2015). Seismic sequence effects on three-dimensional reinforced concrete buildings. *Soil Dynamics and Earthquake Engineering, 72*, 77–88.

Hosseinpour, F., & Abdelnaby, A. (2017). Effect of different aspects of multiple earthquakes on the non-linear behavior of RC structures. *Soil Dynamics and Earthquake Engineering, 92*, 706–725.

Indian Standard, IS 1893. (2002). *Criteria for earthquake resistance design of structures Part-I*. Bureau of Indian Standards.

Indian Standard, IS 456. (2002). *Indian standard plain and reinforced concrete—code of practice*. Bureau of Indian Standards.

Indian Standard, IS 1893. (2016). *Criteria for earthquake resistance design of structures Part-I*. Bureau of Indian Standards.

Kassem, M. M., Nazri, F. M., et al. (2019). Seismic fragility assessment for moment-resisting concrete frame with setback under repeated earthquakes. *Asian Journal of Civil Engineering, 20*(3), 465–477.

Loulelis, D., Hatzigeorgiou, G., et al. (2012). Moment resisting steel frames under repeated earthquakes. *Earthquake and Structures, 3*(3–4), 231–248.

Mander, J. B., Priestley, M. J., et al. (1988). Theoretical stress-strain model for confined concrete. *Journal of Structural Engineering, 114*(8), 1804–1826.

Mohsenian, V., Filizadeh, R., et al. (2021). Seismic performance assessment of eccentrically braced steel frames with energy-absorbing links under sequential earthquakes. *Journal of Building Engineering, 33*, 101576.

Nepal earthquake of 2015, (2015). https://www.britannica.com/topic/Nepal-earthquake-of-2015.

Oyguc, R., Toros, C., et al. (2018). Seismic behavior of irregular reinforced-concrete structures under multiple earthquake excitations. *Soil Dynamics and Earthquake Engineering, 104*, 15–32.

Parekar, S. D., & Datta, D. (2020). Seismic behaviour of stiffness irregular steel frames under mainshock–aftershock. *Asian Journal of Civil Engineering, 21*(5), 857–870.

Park, Y. J., & Ang, A. H. S. (1985). Mechanistic seismic damage model for reinforced concrete. *Journal of Structural Engineering, 111*(4), 722–739.

Raghunandan, M., Liel, A. B., et al. (2015). Aftershock collapse vulnerability assessment of reinforced concrete frame structures. *Earthquake Engineering & Structural Dynamics, 44*(3), 419–439.

SAP2000. (2016). *SI analysis reference manual*. Computer and Structures Inc.

SeismoSoft. (2020). SeismoMatch v.5.1.0 www.seismosoft.com.

Sharma, V., Shrimali, M. K., et al. (2020). Behavior of semi-rigid steel frames under near-and far-field earthquakes. *Steel and Composite Structures, 34*(5), 625–641.

Sharma, V., Shrimali, M. K., et al. (2021). Seismic fragility evaluation of semi-rigid frames subjected to near-field earthquakes. *Journal of Constructional Steel Research, 176*, 106384.

Song, R., Li, Y., et al. (2016). Loss estimation of steel buildings to earthquake mainshock–aftershock sequences. *Structural Safety, 61*, 1–11.

Takeda, T., Sozen, M. A., et al. (1970). Reinforced concrete response to simulated earthquakes. *Journal of the Structural Division, 96*(12), 2557–2573.

Tolentino, D., Flores, R. B., et al. (2018). Probabilistic assessment of structures considering the effect of cumulative damage under seismic sequences. *Bulletin of Earthquake Engineering, 16*(5), 2119–2132.

Zhai, C.-H., Wen, W.-P., et al. (2013). Damage spectra for the mainshock–aftershock sequence-type ground motions. *Soil Dynamics and Earthquake Engineering, 45*, 1–12.

Zhai, C.-H., Wen, W.-P., et al. (2014). The damage investigation of inelastic SDOF structure under the mainshock–aftershock sequence-type ground motions. *Soil Dynamics and Earthquake Engineering, 59*, 30–41.